

1 **1. Introduction**

2 Ongoing development in material and construction technology challenges structural engineers
3 to achieve innovative designs. One of the key issues that they need to address is the fire safety of
4 the designed structure. For example, the evacuation process for high-rise buildings must be
5 carefully considered and the structural safety of the building should be assured. When Reinforced
6 Concrete (RC) columns experience elevated temperatures, their capacities are significantly
7 reduced. This reduction is directly related to the deteriorated mechanical properties of concrete
8 and steel [1]. Fire temperatures also induce nonlinear thermal and transient creep strains [2].

9 The most reliable approach to assess the fire endurance of RC columns is the experimental
10 approach [3], [4]. However, its cost and limitations make it unsuitable for regular design. The
11 capacity of heated RC columns can be analytically assessed using axial force-moment interaction
12 diagrams [5]. Available methods to construct these diagrams include the Eurocode 2 [6] and the
13 Finite Element Method (FE). Eurocode 2 [6] recommends the use of the 500 °C isotherm method.
14 This method assumes that concrete is either undamaged or fully-damaged depending on its
15 temperature as compared to 500 °C. Ignoring concrete damage, when its temperature is lower
16 than 500 °C, can result in unsafe predictions [5], [8]. The FE method can be applied for a range
17 of load eccentricities while varying the applied axial force until failure occurs. Such method
18 needs to be repeated for different fire durations, which makes it computationally expensive [5],
19 [7]. El-Fitiany and Youssef [8], [9], [10] proposed a sectional analysis method that relies on
20 converting the two-dimensional (2D) temperature distribution to an average one-dimensional
21 (1D) temperature distribution to predict the uniaxial behavior of heated sections at different axial
22 load levels (λ). This method can be used in similar manner to the FE method to construct the
23 interaction diagrams. Although it requires much less computational effort, it is still considered

1 unpractical for design engineers.

2 This paper proposes a practical approach to construct the interaction diagrams of RC sections
3 during fire exposure. The proposed approach accounts for the effect of fire on concrete properties
4 and strains. It also eliminates the need to divide the section into smaller elements. The following
5 sections explain the development of an efficient method to calculate an average 1D temperature
6 distribution, the derivation of closed form solutions for concrete internal stresses, and a
7 simplified method to construct the interaction diagrams for fire-exposed columns.

8

9 **2. Interaction diagrams using sectional analysis**

10 Fire temperature decreases concrete and steel mechanical properties and induces thermal and
11 transient strains. A sectional analysis approach suitable for the analysis of rectangular RC
12 sections at elevated temperatures was proposed by El-Fitiany and Youssef [8],[9]. This approach
13 was validated by comparing its results with experimental and analytical work conducted by
14 others. The use of this approach to evaluate the interaction diagrams for a fire-exposed RC
15 section involves the following steps:

16 1. At specific fire duration, the section is divided into a number of elements, Fig. 1a, and the
17 temperature distribution is predicted using the Finite Difference Method (FDM) [1].

18 2. The heat transfer elements are grouped into horizontal layers to conduct sectional analysis.
19 To accurately predict the section behavior, two average temperatures, T_{σ} and T_{avg} , are calculated
20 for each layer. T_{σ} represents the temperature corresponding to the average concrete strength for
21 the layer. T_{avg} represents the algebraic average temperature of the elements within each layer and
22 is suitable to calculate thermal and transient creep strains [9].

23 3. The total concrete strain at elevated temperatures (ϵ) is composed of three terms:

1 unrestrained thermal strain (ε_{th}), instantaneous stress related strain (ε_c), and transient creep
2 strain (ε_{tr}). The total strain is given by Eq. (1).

$$3 \quad \varepsilon = \varepsilon_{th} + \varepsilon_c + \varepsilon_{tr} \quad (1)$$

4 The nonlinear thermal strain (ε_{th}) distribution, Fig. 1f, is calculated using T_{avg} . The thermal
5 strains of the steel bars are calculated based on the concrete temperature at their locations. ε_{th} is
6 then converted to an equivalent linear thermal strain ($\overline{\varepsilon_{th}}$), Fig. 1c, by considering self-
7 equilibrium of internal thermal forces in concrete and steel layers. $\overline{\varepsilon_{th}}$ is represented by the value
8 of the axial strain (ε_i). The corresponding curvature is equal to zero as the section is assumed to
9 be heated from four faces. Fig. 1e shows the differences between the equivalent linear and
10 nonlinear thermal strains, which represent the self-induced thermal strains (ε_{st}). These strains are
11 assigned as initial strains for the concrete and steel layers to model the corresponding self-
12 induced self-equilibrating thermal stresses. The terms ε_{st} , ε_c , and ε_{tr} are lumped into an
13 equivalent mechanical strain ε_{cT} as shown by Eq. (2).

$$14 \quad \varepsilon = \overline{\varepsilon_{th}} + (\varepsilon_{st} + \varepsilon_c + \varepsilon_{tr}) = \overline{\varepsilon_{th}} + \varepsilon_{cT} \quad (2)$$

15 4. For assumed top strain and curvature, the corresponding stresses in the concrete and steel
16 layers are evaluated using the constitutive stress-strain relationships of concrete and steel that
17 were recommended by Youssef and Mofteh [2] can evaluate. The developed internal forces and
18 the corresponding axial force are then calculated. This process is repeated for different top strains
19 until the desired axial force and the corresponding moment are obtained. This process is repeated
20 for different curvature values, which allows sketching the moment-curvature relationship, Fig. 2.
21 The maximum applied moment defines the moment of resistance at the assumed axial load.

22 5. Repeating step 4 for different axial load levels (λ) allows evaluating the interaction diagram
23 for the given section at a given fire duration.

1 6. Steps 1 to 5 are to be repeated at different fire durations.

2 Two potential simplifications to the described method are to ignore ε_{st} and use T_{avg} for
3 strength calculations. The errors corresponding to such simplifications are assessed in this section
4 by analyzing the columns shown in Table 1 at different axial load levels ($\lambda = 0.0 - 0.9$).
5 Comparisons between the analytical flexural capacities with and without the mentioned
6 simplifications are shown in Figs. 3 and 4. It is clear that ignoring ε_{st} or using T_{σ} for stress
7 calculations have negligible effect on the flexural capacity of the examined columns. These
8 simplifications might not be appropriate while examining the column deformations.

9 Although the sectional analysis method is relatively easy to apply as compared to the FE
10 method, it requires knowledge of heat transfer principles and the ability to conduct iterative
11 analysis at elevated temperatures. The following sections present a simplified approach to predict
12 the interaction diagram of a RC column during fire exposure.

13

14 **3. Proposed method**

15 Concrete has low thermal conductivity, which results in a steep temperature distribution near
16 the heated faces and a constant temperature at the core of the heated section. Thus, the concrete
17 strength becomes variable near the heated faces and constant within the inner core. The flexural
18 capacity of the section can be estimated by equilibrating the internal compression and tension
19 forces in concrete and steel. A number of approximations are assumed to allow integrating
20 concrete stress-strain relationships with respect to mechanical strain and temperature
21 distributions. The main assumptions include:

22 1) using a 1D average temperature distribution, i.e. T_{avg} , instead of 2D elevated temperature
23 contours within the RC sections,

- 1 2) choosing an appropriate, i.e. integrable, algebraic function to represent T_{avg} variation along
- 2 the section height,
- 3 3) ignoring the effect of self-induced strain, ε_{st} , on the flexural capacity of fire-exposed
- 4 columns,
- 5 4) using an integratable stress-strain constitutive relationships for concrete at elevated
- 6 temperatures, and
- 7 5) identifying the envelope for concrete failure strain by plotting the variation of maximum
- 8 strain ($\varepsilon_{cT max}$) along section height.

9 For a given fire duration and axial load, the proposed method provides simplified equations to
10 evaluate: (1) a one-dimensional average temperature distribution, (2) the concrete strains at
11 failure, (3) the concrete and steel stresses at failure, and (4) the flexural capacity of the section.
12 The following sections provide the derivations of the simplified equations.

13

14 **4. Average temperature distribution**

15 In this section, a simplified method to calculate the temperature distribution within a fire-
16 exposed concrete section is presented. The section is then divided into regions of constant and
17 variable temperatures. Equations to evaluate the average temperature (T_{avg}) profile are derived.

18

19 *4.1. Wickstrom simplified formulas*

20 Wickstrom [11] proposed and validated a set of handy formulas to calculate the 2D
21 temperature distribution within a fire exposed concrete section. Wickstrom's formulas can be
22 applied for any type of concrete and fire scenario. However, they are practically easy for ISO 834
23 standard fire and normal weight concrete. Wickstorm's formulas do not account for variability in

1 the thermal conductivity of concrete, moisture content, and nonlinear boundary conditions that
 2 have prescribed temperatures and heat fluxes [11]. Concrete initial moisture content has a
 3 negligible effect on the temperature predictions [1]. Assuming a constant thermal conductivity for
 4 the concrete material, accurate predictions of the temperature variation within a cross-section can
 5 be obtained [11].

6 Fig. 5 shows a RC concrete column subjected to fire from four sides; Left (L), Right (R),
 7 Bottom (B), and Top (T) faces. Application of Wickstrom's formulas to calculate the temperature
 8 distribution within this section can be summarized as follows:

9 1) The fire temperature T_f in Celsius is first calculated at a specific fire duration t (hr) using an
 10 assumed fire temperature-time relationship.

11 2) An equivalent ISO 834 fire duration (t^*) is then calculated. t^* evaluates the corresponding
 12 time of exposure to the standard ISO 834 standard fire to have a temperature of T_f . The ratio
 13 between the modified time (t^*) and the actual fire duration (t) defines a dimensionless
 14 compartment time factor (Γ). The ISO 834 standard fire can be described by Eq. (3).

$$15 \quad T_f = 345 \log(480 t^* + 1) \quad (3)$$

16 where T_f is the ISO 834 standard fire temperature in Celsius at a modified fire duration t^* in hrs.

17 3) The temperature rise at any point (x, y) within the section due to heating from four sides can
 18 be estimated using Eq. (4).

$$19 \quad T_{xy} = [n_w (n_x + n_y - 2n_x \cdot n_y) + n_x \cdot n_y] T_f \quad (4a)$$

$$20 \quad n_w = 1 - 0.0616 (\sqrt{\Gamma} \cdot t)^{-0.88} \geq 0.0 \quad (4b)$$

$$21 \quad n_x = \left[0.18 \ln \left(\frac{t}{x^2} \right) - 0.81 \right]_{\text{Fire (L)}} + \left[0.18 \ln \left(\frac{t}{(b-x)^2} \right) - 0.81 \right]_{\text{Fire (R)}} \geq 0.0 \quad (4c)$$

$$22 \quad n_y = \left[0.18 \ln \left(\frac{t}{y^2} \right) - 0.81 \right]_{\text{Fire (B)}} + \left[0.18 \ln \left(\frac{t}{(h-y)^2} \right) - 0.81 \right]_{\text{Fire (T)}} \geq 0.0 \quad (4d)$$

1 where b is the section width, h is the section height, T_{xy} is the temperature rise at any point (x ,
 2 y) in Celsius, n_w is the ratio between the surface temperature and the fire temperature, and n_x
 3 and n_y are the ratios between the internal and surface temperatures considering heating in the x
 4 and y directions, respectively. Wickstrom's formula, Eq. (4), is extended in the following
 5 subsections to obtain an average 1D temperature distribution along the section depth, i.e. y -axis.

6

7 4.2. Temperature regions

8 Figs. 5 and 6 show the potential temperature regions, R1, R2, and R3, within a concrete
 9 section. The values shown in each region indicate the heating surface causing temperature
 10 variation in x and y directions. Values of zero indicate that the temperature is constant in a given
 11 direction. While region R2(0,0), Fig. 5, has a constant temperature, region R3(L+R, T+B), Fig.
 12 6, has variable temperature that is affected by the fire temperature of the four sides. The value z
 13 defines the boundaries of the temperature regions and can be evaluated by equating n_x or n_y ,
 14 Eqs. (4c) or (4d), to zero. This will result in Eq. (5). Value of z is less than $b/2$ and $h/2$ in Fig. 5
 15 and is greater than them in Fig. 6.

$$16 \quad z = \sqrt{e^{-4.5} t} \quad (5)$$

17 The schematic temperature profiles across lines 1-1 and 2-2 of Fig. 5 present the variation
 18 of temperature in x direction at $y \leq z$ and $y = z \rightarrow (h/2 - z)$, respectively. Both profiles show
 19 varying temperature for R1 and constant temperature for R2. The schematic temperature profiles
 20 for lines 1-1 and 2-2 of Fig. 6 present the variation of temperature in the x direction at $y \leq (h -$
 21 $z)$ and $y = (h - z) \rightarrow z$, respectively. All regions have variable temperature profile.

22

23

1 4.3. Average temperatures

2 Eq. (4) predicts the temperature rise at different locations within the studied concrete
3 section. For each of lines 1-1 and 2-2, n_y is constant and n_x value defines the temperature along
4 the line. Three equations are derived to evaluate the average temperature within each region at a
5 given y value. $T_{avg 1}$, Eq. (6a), represents the average temperature for regions affected by heating
6 from either L or R. $T_{avg 2}$, Eq. (6b), represents the average temperature for regions not affected
7 by heating from L or R. $T_{avg 3}$, Eq. (6c), represents the average temperature due to heating from
8 the left and right sides simultaneously, i.e. (L + R).

$$9 \quad T_{avg 1} = [0.18 n_w - 0.36 n_w \cdot n_y + 0.18 n_y] \left[x_2 \ln \left(\frac{t}{x_2^2} \right) - x_1 \ln \left(\frac{t}{x_1^2} \right) \right] \frac{T_f}{(x_2 - x_1)} \\
10 \quad -0.45 T_f \cdot n_w + 1.9 T_f \cdot n_w \cdot n_y - 0.45 T_f \cdot n_y \quad x = x_1 \rightarrow x_2 \quad (6a)$$

$$11 \quad T_{avg 2} = T_f \cdot n_w \cdot n_y \quad (6b)$$

$$12 \quad T_{avg 3} = (0.18 n_w + 0.18 n_y - 0.36 n_w \cdot n_y) \left[\ln \left(\frac{t}{(b-x_2)^2} \right) x_2 - \ln \left(\frac{t}{(b-x_1)^2} \right) x_1 \right] \frac{T_f}{(x_2 - x_1)} \\
13 \quad + b (0.36 n_w \cdot n_y - 0.18 n_w - 0.18 n_y) \left[\ln \left(\frac{t}{(b-x_2)^2} \right) - \ln \left(\frac{t}{(b-x_1)^2} \right) \right] \frac{T_f}{(x_2 - x_1)} \\
14 \quad -0.45 T_f \cdot n_w + 0.9 T_f \cdot n_w \cdot n_y - 0.45 T_f \cdot n_y + T_{avg 1} \quad x = x_1 \rightarrow x_2 \quad (6c)$$

15 The average temperatures, $T_{avg 1}$, $T_{avg 2}$, and $T_{avg 3}$, are shown in Figs. 5 and 6 by the
16 dashed lines. The ambient temperature (20 °C) is to be added to the calculated average
17 temperatures. A weighted average temperature can then be calculated for each line to facilitate
18 sketching the final average temperature distribution along the section height as shown in Figs. 5
19 and 6. The final temperature profile can be idealized using Eq. (7). z_1 and z_2 are constants that
20 can be estimated using the weighted average temperature values at $y = 0.0$ and $y = z$. This
21 equation form was chosen as it allows reaching a closed form solution.

$$22 \quad T_{avg} = z_1 \cdot e^{(z_2 \cdot y)} \quad (7)$$

1 where $z_1 = T_{avg}(y=0.0)$ and $z_2 = \frac{\ln\left[\frac{T_{avg}(y=z)}{z_1}\right]}{z}$

2

3 **5. Concrete and steel constitutive relationships**

4 Concrete and steel models used in the proposed method are discussed in this section.

5

6 *5.1. Concrete compressive strength*

7 Concrete compressive strength experiences significant degradation at elevated
8 temperatures. Eurocode 2 predicts the reduced compressive strength (f'_{cT}) for siliceous and
9 carbonate concretes as a ratio from its ambient value (f'_c) [6]. The reduction in f'_{cT} for siliceous
10 concrete can be fitted by a polynomial equation, Eq. (8). Fig. 7 shows the flexural capacities of
11 the columns in Table 1 considering either siliceous or carbonate concrete. Carbonate aggregate
12 slightly increases the flexural capacity of RC columns during fire exposure, and, thus the use of
13 Eq. (8) can be conservatively applied for carbonate aggregate concrete.

$$14 \quad f'_{cT} / f'_c = 1.76 \times 10^{-9} T_{avg}^3 - 3 \times 10^{-6} T_{avg}^2 + 2.5 \times 10^{-4} T_{avg} + 1.00 \quad (8)$$

15 where T_{avg} is the weighted average temperature, in °C, calculated in the previous section.

16

17 *5.2. Thermal strains*

18 The total concrete strain at elevated temperatures (ε) is given by Eq. (2). The thermal
19 curvature shifts the $M-\psi$ diagrams, Fig. 2. The flexural capacity is not affected by the thermal
20 deformations, which allows ignoring $\overline{\varepsilon_{th}}$ while calculating the section capacity.

21

22

1 5.3. Concrete strain at peak stress

2 The value of ε_c at the peak stress (f'_{cT}), i.e. ε_{oT} , defines the stress-strain relationship
3 during fire exposure, Fig. 8. For loaded RC columns, the effect of elevated temperatures on ε_{oT}
4 is negligible [2]. Fig. 9 shows the variation of $\varepsilon_{oT} + \varepsilon_{tr}$ with fire temperature as proposed by
5 Eurocode 2. The shown values of $\varepsilon_{oT} + \varepsilon_{tr}$ are consistent with Terro's model [10] within its
6 validated temperature range, i.e. up to 600 °C. A linear relationship, Eq. (9), is chosen to
7 represent the Eurocode 2 recommendation. Such a relationship allows reaching a closed form
8 solution while accounting for concrete nonlinearity as will be discussed in the next section. To
9 evaluate the error associated with using this approximation, the flexural capacities, at different
10 axial load levels ($\lambda = 0.0 - 0.9$), of the columns shown in Table 1 are calculated up to 4 hrs of
11 ASTM-E119 standard fire exposure. Fig. 10 shows that this approximation has a minor effect on
12 the flexural capacity predictions.

$$13 \varepsilon_{oT} + \varepsilon_{tr} = 2.52 \times 10^{-5} T_{avg} \quad 80 \text{ °C} < T_{avg} \leq 1200 \text{ °C} \quad (9)$$

14

15 5.4. Concrete ultimate strain

16 Concrete ultimate strain is the strain at which concrete crushing occurs. Elevated
17 temperatures increase this strain. Models evaluating the effect of elevated temperatures on the
18 ultimate concrete compressive strain (ε_{uT}) are limited in the literature. Meda et al. [13] assumed
19 that ε_{uT} corresponds to a maximum post peak stress of $0.85 f'_{cT}$. ε_{uT} is defined in Eurocode 2 as
20 the strain corresponding to zero compression stress and can be calculated using Eq. (10). The
21 difference between ε_{uT} and $\varepsilon_{oT} + \varepsilon_{tr}$ is constant and equal to 0.02.

$$22 \varepsilon_{uT} = 2.52 \times 10^{-5} T_{avg} + \Delta\varepsilon = \varepsilon_{oT} + \varepsilon_{tr} + 0.02 \quad (10)$$

23

1 5.5. Maximum concrete strain

2 The maximum concrete strain is defined as the strain corresponding to the maximum
3 moment resistance. As shown in Fig. 2, this strain is usually lower than ε_{uT} . Elbahy et al. [14]
4 studied the variation of this strain with the axial load level at ambient temperature.

5 A parametric study is conducted to evaluate the compression strain ($\varepsilon_{cT\ max}$)
6 corresponding to the flexural capacity at elevated temperatures, i.e. peak points in Fig. 2. The
7 flexural capacities of the columns shown in Table 1 considering different axial load levels ($\lambda =$
8 $0.0 - 0.9$) were evaluated. For each column section, the $M-\psi$ diagrams are constructed assuming
9 different lengths for the descending branch of the concrete stress-strain curve ($r \cdot \Delta\varepsilon$), Fig. 8. r
10 values of 0.00, 0.25, 0.50, 0.75, and 1.0 are assumed. Fig. 11 shows the interaction diagrams for
11 column C2 at 1.0 hr ASTM-E119 fire exposure. The dashed line represents the correct flexural
12 capacities as determined by the peak points of the constructed $M-\psi$ diagrams at different axial
13 loads. Ignoring the descending branch, $r = 0.00$, results in conservative flexural capacity. On
14 the other hand, considering the full descending branch, i.e. $r = 1.0$, significantly underestimates
15 the flexural capacity. Fig. 12 shows a comparison between the correct flexural capacities and the
16 predicted flexural capacities considering $r = 0.00, 0.25, \text{ and } 0.5$ for all of the analyzed columns
17 for fire durations up to 4.0 hrs. Reasonable predictions are obtained when r is taken equal to
18 0.25. Thus, $\varepsilon_{cT\ max}$, Eq. (11), is defined by adding 0.25 $\Delta\varepsilon$ to $(\varepsilon_{oT} + \varepsilon_{tr})$, where $\Delta\varepsilon$ equals to
19 0.02.

$$20 \varepsilon_{cT\ max} = (\varepsilon_{oT} + \varepsilon_{tr}) + 0.005 \quad (11)$$

21

22 5.6. Concrete stress-strain relationships

23 The relationship between the compression stress, f_{cT} , and the corresponding mechanical

1 strain, ε_{cT} , at elevated temperatures was studied by a number of researchers. A general and
2 simple approach to estimate the $f_{cT} - \varepsilon_{cT}$ descending branch is proposed by Eurocode 2 and
3 represented by Eq. (12). This curve is adopted in this study due to its simplicity and ease of
4 implementation in the proposed method. Eq. (12) implicitly accounts for transient creep as the
5 strain corresponding to the maximum concrete stress is shifted using the transient creep strain.
6 Fig. 8 shows the application of Eq. (12) at three average temperatures ($T_{avg} = 200, 400,$ and
7 600 °C). Eqs. (8) and (9) are used to calculate f'_{cT}/f'_c and $(\varepsilon_{oT} + \varepsilon_{tr})$, respectively.

$$8 \quad f_{cT} = f'_{cT} \left[2 \left(\frac{\varepsilon_{cT}}{\varepsilon_{oT} + \varepsilon_{tr}} \right) - \left(\frac{\varepsilon_{cT}}{\varepsilon_{oT} + \varepsilon_{tr}} \right)^2 \right] \quad \varepsilon_{cT} \leq (\varepsilon_{oT} + \varepsilon_{tr}) \quad (12a)$$

$$9 \quad = f'_{cT} \left[\frac{\varepsilon_{uT} - \varepsilon_{cT}}{0.02} \right] \quad (\varepsilon_{oT} + \varepsilon_{tr}) < \varepsilon_{cT} \leq \varepsilon_{uT} \quad (12b)$$

10

11 5.7. Steel stress-strain relationships

12 Lie et al.'s model [1] is used to predict the reduced yield strength of reinforcing bars
13 (f_{yT}), Eq. (13), and the stress-strain ($f_{sT} - \varepsilon_{sT}$) relationship, Eq. (14).

$$14 \quad f_{yT} = \left[1 + \frac{T}{900 \ln(T/1750)} \right] f_y \quad 0 < T \leq 600 \text{ °C} \quad (13a)$$

$$15 \quad = \left[\frac{340 - 0.34 T}{T - 240} \right] f_y \quad 600 < T \leq 1000 \text{ °C} \quad (13b)$$

$$16 \quad f_{sT} = \frac{f[T, 0.001]}{0.001} \varepsilon_{sT} \quad \varepsilon_{sT} \leq \varepsilon_p \quad (14a)$$

$$17 \quad f_{sT} = \frac{f[T, 0.001]}{0.001} \varepsilon_p + f [T, (\varepsilon_{sT} - \varepsilon_p + 0.001)] - f [T, 0.001] \quad \varepsilon_{sT} > \varepsilon_p \quad (14b)$$

$$18 \quad \varepsilon_p = 4 \times 10^{-6} f_y \quad (14c)$$

$$19 \quad f [T, 0.001] = (50 - 0.04 T) \left[1 - e^{(-30 + 0.03 T) \sqrt{0.001}} \right] \times 6.9 \quad (14d)$$

$$20 \quad f [T, (\varepsilon_{sT} - \varepsilon_p + 0.001)] = (50 - 0.04 T) \left[1 - e^{(-30 + 0.03 T) \sqrt{(\varepsilon_{sT} - \varepsilon_p + 0.001)}} \right] \times 6.9 \quad (14e)$$

1 **6. Evaluation of Concrete Internal Forces**

2 The following sections propose a simplified approach to calculate concrete internal forces
3 using the predicted T_{avg} distribution and the presented material models.

5 *6.1. Concrete strain profile*

6 The average temperature profile (T_{avg}), Eq. (7), is a function of the distance y . Utilizing
7 the predicted T_{avg} distribution, $(\varepsilon_{oT} + \varepsilon_{tr})$ and $\varepsilon_{cT\ max}$ distributions can be evaluated using Eqs.
8 (9) and (11), respectively. Fig. 13 shows these distributions for the column section shown in Fig.
9 5. A linear ε_{cT} distribution is assumed as given by Eq. 15.

$$10 \quad \varepsilon_{cT} = z_3 y + z_4 \quad (15)$$

11 where z_3 and z_4 are constants that define ε_{cT} variation in y direction.

12 The flexural capacity occurs when ε_{cT} value at any height y is equal to $\varepsilon_{cT\ max}$ at the
13 same height. Three possible failure scenarios should be considered:

14 1) concrete fails at extreme top fibers of the section, i.e. $y = h$. The slope of ε_{cT} distribution (z_3)
15 can take any value between zero (horizontal line) and the slope of the tangent to $\varepsilon_{cT\ max}$ profile at
16 $y = h$, Fig. 13.

17 2) concrete fails at the boundaries of the constant T_{avg} zone, i.e. $y = h - z$. The slope of ε_{cT}
18 distribution (z_3) can take any value between infinity (vertical line) and the slope of the tangent of
19 $\varepsilon_{cT\ max}$ profile at $y = h - z$.

20 3) concrete fails at any point between $y = h - z$ and $y = h$. In this case, ε_{cT} distribution is
21 tangent to $\varepsilon_{cT\ max}$ profile.

22

23

1 6.2. Calculation of concrete internal forces and their locations

2 Average concrete compressive stresses $(f_{cT})_{avg}$ that correspond to ε_{cT} profile can be
3 estimated using Eq. (12). These stresses are integrated over the section area to calculate the
4 internal compression force in concrete (C_c) and its location (y), Eqs. (16) and (17).

$$5 C_c = \int_{y=(h-c)}^h (f_{cT})_{avg} b dy \quad (16)$$

$$6 C_c \cdot y = \int_{y=(h-c)}^h (f_{cT})_{avg} b y dy \quad (17)$$

7 where b and h are the section width and depth (m), respectively and c is the neutral axis depth
8 (m). $(f_{cT})_{avg}$ is the average concrete compressive stress (kPa) at different y values.

9 The following substitutions are made in Eqs. (16) and (17) to allow reaching a closed
10 form solution: (1) $(f_{cT})_{avg} = \text{Eq. (12)}$, (2) $(\varepsilon_{oT} + \varepsilon_{tr}) = \text{Eq. (9)}$, (3) $f'_{cT} = \text{Eq. (8)}$, (4) $\varepsilon_{uT} =$
11 Eq. (10) , (5) $T_{avg} = \text{either a constant value or Eq. (7)}$, and (6) $\varepsilon_{cT} = \text{Eq. (15)}$. The solutions are
12 given by Eqs. (18) to (25), which are shown in the Appendix. For values of $\varepsilon_{cT} \leq (\varepsilon_{oT} + \varepsilon_{tr})$,
13 two equations are given for the compressive force in concrete, Eqs. (18) and (22). They allow
14 evaluating $C_{c o(v)}$ and $C_{c o(c)}$ for variable and constant T_{avg} distributions, respectively. The
15 centroids of these compressive forces are given by Eqs. (19) and (23). For values of $\varepsilon_{cT} > (\varepsilon_{oT} +$
16 $\varepsilon_{tr})$, the compressive force in concrete, $C_{c u(v)}$ or $C_{c u(c)}$, can be evaluated using Eqs. (20) and
17 (24) for variable or constant T_{avg} distributions. The centroids of these forces are given by Eqs.
18 (21) and (25).

19 Fig. 13 shows a four-face heated RC column section with two potential mechanical strain
20 (ε_{cT}) distributions. The magnitude and location of $C_{c o(v)}$, Fig. 13a, are evaluated using Eqs. (18)
21 and (19), respectively. The magnitude and location of $C_{c u(v)}$ are evaluated using Eqs. (20) and
22 (21), respectively. The magnitude and location of $C_{c o(c)}$, Fig. 13b, are evaluated using Eqs. (22)

1 and (23), respectively. The magnitude and location of $C_{cu(c)}$ are evaluated using Eqs. (24) and
2 (25), respectively. The total internal compression force $C_{co(c)}$ is calculated by summing two or
3 more components shown in Fig. 13.

5 6.3. Interaction Diagram

6 The interaction diagram for a fire-exposed RC column can be constructed using the
7 following main steps. At specific fire duration,

8 1) an external axial load (P_{app}) is assumed.

9 2) an average temperature (T_{avg}) distribution is predicted using Eq. (7). Based on T_{avg}
10 distribution, $(\varepsilon_{oT} + \varepsilon_{tr})$ and $\varepsilon_{cT max}$ distributions are evaluated using Eqs. (9) and (11)

11 3) different linear mechanical strain (ε_{cT}) distributions are assumed, i.e. varying z_3 and z_4 in Eq.
12 (15). For each ε_{cT} distribution, Eqs. (18) to (25) are used to calculate the corresponding
13 concrete force and its location. Equilibrium is then conducted between internal forces in
14 concrete and steel and the assumed external axial load, P_{app} . An iterative procedure requires
15 changing z_3 and z_4 till force equilibrium is achieved.

16 4) the corresponding flexural capacity is calculated.

17 5) The above steps are repeated considering different axial loads and the corresponding flexural
18 capacities are evaluated. These capacities define the interaction diagram of the analyzed
19 column section at specific fire duration.

20

21 7. Illustrative Example

22 The 600 mm square column analyzed by Meda et al. [13], Fig. 14a, is used as an example
23 to explain the proposed method. The column is reinforced by 24 – 20 mm steel bars uniformly

1 distributed with 40 mm concrete cover to main reinforcement. The compressive and yield
2 strength of the siliceous concrete and reinforcing bars are 40 MPa and 430 MPa, respectively.
3 The column is subjected to a standard ISO 834 fire from four directions.

4 Sectional analysis was first used to predict the interaction diagram after $t =$
5 0.0 hr, 1.5 hrs, and 3.0 hrs of fire exposure. The FDM mesh used for the heat transfer
6 calculations, by Lie et al. [1], is shown in Fig. 14a. The corresponding average temperature
7 distribution is shown in Fig. 14b as discrete points [1]. The interaction diagrams shown in Fig. 15
8 were constructed using the iterative method mentioned in section 2.

9 The proposed simplified method is used to predict the interaction diagram for the column
10 section after $t = 1.5$ hrs of fire exposure. A simple excel spreadsheet was prepared to apply the
11 following steps of the proposed method.

12 1) ISO 834 fire temperatures T_f of 986 °C is calculated using Eq. (3). Γ is equal to 1.

13 2) n_w value of 0.96 is estimated using Eq. (4b).

14 3) z value of 0.129 for t of 1.5 hrs is calculated using Eq. (5). Fig. 16 shows the different regions
15 of the example column.

16 4) The average temperatures for each region are calculated as follows,

17 z value of 0.129 is used to define the region boundaries. Substituting in Eq. (6a) using $x_1 =$
18 0.0 m, and $x_2 = 0.129$ m results in $T_{avg\ 1} = 320 + 619 n_y$. Substituting in Eq. (6b) results
19 in $T_{avg\ 2} = 923 n_y$.

20 5) The ambient temperature (20 °C) is added to the calculated average temperatures. Weighted
21 average temperatures are then calculated at different values of y . The average temperature
22 distribution is shown in Fig. 14b as a solid line. The figure shows that the values calculated
23 using the developed simplified method matches the values predicted using the FDM method.

- 1 6) The constants (z_1 and z_2) of Eq. (7) are evaluated using values of T_{avg} at y_1 of 0.0 m and
2 y_2 of 0.129 m.
- 3 The predicted T_{avg} distribution is used to plot $(\varepsilon_{oT} + \varepsilon_{tr})$ and $\varepsilon_{cT\ max}$ distributions along y
4 direction using Eqs. (9) and (11), respectively, Fig. 17b.
- 5 7) A strain distribution is assumed as shown by the heavy line in Fig. 17b (z_3 and z_4 of Eq. (15)
6 are equal to 0.089 and -0.033 , respectively). The line is tangent to the concrete crushing
7 curve, which assumes that concrete crushing occurs at the point highlighted in Fig. 17b.
- 8 8) concrete compressive forces and corresponding centroids are calculated using expressions
9 provided in Appendix I as follows:
- 10 a. For $y = 0.374 \rightarrow 0.421\ m$ [constant temperature and $\varepsilon_{cT} \leq (\varepsilon_{oT} + \varepsilon_{tr})$]
11 Eqs. (22) and (23) $\rightarrow C_{c\ o\ (c)} = -745,905\ N$, $C_{c\ o\ (c)} \cdot y = -301\ kN \cdot m$ (i.e. $y =$
12 $0.404\ m$)
- 13 b. For $y = 0.421 \rightarrow 0.471\ m$ [constant temperature and $\varepsilon_{cT} > (\varepsilon_{oT} + \varepsilon_{tr})$]
14 Eqs. (24) and (25) $\rightarrow C_{c\ u\ (c)} = -1,014,715\ N$, $C_{c\ u\ (c)} \cdot y = -452\ kN \cdot m$ (i.e. $y =$
15 $0.445\ m$)
- 16 c. For $y = 0.471 \rightarrow 0.581\ m$ [variable temperature and $\varepsilon_{cT} > (\varepsilon_{oT} + \varepsilon_{tr})$]
17 Eqs. (20) and (21) $\rightarrow C_{c\ u\ (v)} = -1,520,285\ N$, $C_{c\ u\ (v)} \cdot y = -789\ kN \cdot m$ (i.e. $y =$
18 $0.519\ m$)
- 19 d. For $y = 0.581 \rightarrow 0.600\ m$ [variable temperature and $\varepsilon_{cT} \leq (\varepsilon_{oT} + \varepsilon_{tr})$]
20 Eqs. (18) and (19) $\rightarrow C_{c\ o\ (v)} = -60,833\ N$, $C_{c\ o\ (v)} \cdot y = -36\ kN \cdot m$ (i.e. $y =$
21 $0.592\ m$)
- 22 9) The temperature of steel bars in the example column can be calculated using the Wickstrom
23 method, Eq. (4a). The calculated temperatures for steel bars are given in Table 2.

1 10) The steel stresses are calculated using Eq. (14) and given in Table 2.

2 11) The calculated concrete and steel forces are in equilibrium with external forces. The flexural
3 capacity of the example column is predicted after 1.5 *hr* ISO 834 fire exposure as
4 957 *kN.m*. The corresponding applied axial load (P_{app}) is calculated by summing the
5 internal forces in concrete and steel (P_{app} is 3,000 *kN*).

6 The proposed method is repeated for the example RC column using different ϵ_{cT}
7 distributions. The flexural capacity and corresponding axial load are calculated for each
8 distribution. Fig. 15 shows the interaction diagrams for the example column at 1.5 *hr* and 3 *hrs*
9 fire exposures. The proposed method's predictions and the sectional analysis method results are
10 in a good match, Figs. 15 and 18. Meda et al. [13] overestimates the flexural capacity at $t = 0.0$
11 *hrs*. This can be due to the used approximate concrete stress-strain relationship [13].

12

13 **8. Validation**

14 The proposed method is validated in this section by comparing its results with analytical
15 and experimental results by others.

16

17 *8.1. Law and Gillie (2010)*

18 Fig. 19 shows a rectangular RC section subjected to a standard ISO 834 fire from three
19 sides. Law and Gillie [5] constructed, using sectional analysis, the interaction diagrams for this
20 section at $t = 1$ *hr* and 2 *hrs*. A comprehensive finite element analysis was conducted by Law
21 and Gillie to validate the results of the sectional analysis method [5]. The distortion in the
22 interaction diagrams is due to the change of plastic centroid location as a result of the uneven
23 heating of the section during fire exposure. The proposed method is applied as explained in the

1 illustrative example. The effect of uneven heating, i.e. three sides only, is considered as follows
2 1) The z value is calculated, using Eq. (5), for the bottom side only. The weighted average
3 temperatures are calculated at y equals to 0.0 and z . The corresponding constants (z_1 and z_2)
4 of Eq. (7) are evaluated for this region of the heated section. The average temperature
5 distribution is variable at $y \leq z$ and uniform at $y > z$.
6 2) The asymmetric T_{avg} distribution is used to plot $(\epsilon_{oT} + \epsilon_{tr})$ and $\epsilon_{cT max}$ distributions along y
7 direction using Eqs. (9) and (11), respectively. The predicted $(\epsilon_{oT} + \epsilon_{tr})$ and $\epsilon_{cT max}$
8 distributions are asymmetric as well, i.e. variable at $y \leq z$ and uniform at $y > z$. The concrete
9 compressive forces and corresponding centroids are calculated similar to the illustrative
10 example using expressions provided in Appendix I.

11 As shown in Figs. 18 and 20, the proposed method results are in close agreement with the
12 results of Law and Gillie.

13

14 8.2. Lie and Wollerton (1986)

15 Fig. 21a shows the cross-section and reinforcement for a RC column tested by Lie and
16 Wollerton [3]. The tested column was subjected to a standard ASTM-E119 fire exposure under
17 25 mm eccentric load ($P = 1,000 kN$), which was kept constant during the whole test. The fire
18 endurance recorded at the end of the fire test was 181 min ($t = 3.0 hrs$). The reinforcing steel
19 cover was 48 mm and the end conditions of the tested column were pinned-pinned. Fig. 21b
20 shows the predicted T_{avg} distribution through the section height. T_{avg} distribution does not
21 include a constant distribution due to heating overlap from the top and bottom faces. Based on
22 T_{avg} distribution, $(\epsilon_{oT} + \epsilon_{tr})$ and $\epsilon_{cT max}$ profiles are calculated and are shown in Fig. 21b. A
23 linear ϵ_{cT} distribution is then assumed, Fig. 21c, i.e. concrete crushing occurs at top fibers of the

1 section. The internal forces and moments for concrete and steel are calculated using the equations
2 provided in the appendix. Fig. 21d shows the values for internal concrete compressive forces and
3 their locations. By conducting equilibrium between external and internal forces, the proposed
4 method estimates a 25 mm eccentric load capacity of 890 kN, i.e. a small error of -11%.

6 **9. Summary and Conclusions**

7 Interaction diagrams represent an efficient tool to predict the flexural capacity of RC
8 columns at ambient and fire conditions. Sectional analysis method can be used to construct
9 interaction diagrams for fire exposed RC columns. However, it is computationally expensive for
10 design engineers as it requires dividing the column section into layers to conduct heat transfer
11 and stress analysis during fire exposure. A simple technique to calculate an average 1D
12 temperature distribution is presented and validated in this paper. Based on this temperature
13 distribution, the heated RC section is divided into different zones to conduct stress analysis. A
14 number of approximations are assumed to allow integrating concrete stress-strain relationships
15 with respect to mechanical strain and temperature distributions.

16 Mathematical expressions are then derived to calculate the internal compressive forces
17 and their locations. Structural engineers can use these expressions to easily construct the
18 interaction diagrams for fire exposed RC columns using first principles. The predictions of the
19 proposed method are in good agreement with analytical and experimental results by others.

20

1 Nomenclature

2	A_1	factor used in calculating internal concrete force, equals to $e^{y_1 z_2}$
3	A_2	factor used in calculating internal concrete force, equals to $e^{y_2 z_2}$
4	b	column width in x direction
5	C_c	internal compression force in concrete
6	$C_{c o(v)}$	concrete compression force at $\varepsilon_{cT} \leq (\varepsilon_{oT} + \varepsilon_{tr})$ for variable T_{avg} distribution
7	$C_{c o(v)} \cdot y$	concrete moment about x axis at $\varepsilon_{cT} \leq (\varepsilon_{oT} + \varepsilon_{tr})$ for variable T_{avg} distribution
8	$C_{c u(v)}$	concrete compression forces at $\varepsilon_{cT} > (\varepsilon_{oT} + \varepsilon_{tr})$ for variable T_{avg} distribution
9	$C_{c u(v)} \cdot y$	concrete moment about x axis at $\varepsilon_{cT} > (\varepsilon_{oT} + \varepsilon_{tr})$ for variable T_{avg} distribution
10	$C_{c o(c)}$	concrete compression force corresponding to $\varepsilon_{cT} \leq (\varepsilon_{oT} + \varepsilon_{tr})$ for constant T_{avg}
11	$C_{c o(c)} \cdot y$	concrete moment about x axis at $\varepsilon_{cT} \leq (\varepsilon_{oT} + \varepsilon_{tr})$ for constant T_{avg}
12	$C_{c u(c)}$	concrete compression force corresponding to $\varepsilon_{cT} > (\varepsilon_{oT} + \varepsilon_{tr})$ for constant T_{avg}
13	$C_{c u(c)} \cdot y$	concrete moment about x axis at $\varepsilon_{cT} > (\varepsilon_{oT} + \varepsilon_{tr})$ for constant T_{avg}
14	f'_c	compressive strength for concrete at ambient temperature
15	f_y	yield strength of steel bars at ambient temperature
16	f'_{cT}	reduced compressive strength at elevated temperatures
17	f_{cT}	compression stress in heated concrete
18	f_{yT}	reduced yield strength of reinforcing bars at elevated temperatures
19	f_{sT}	compression or tension stress in heated steel bars
20	$(f_{cT})_{avg}$	average concrete compressive stresses
21	h	cross-section height
22	M	flexural moment
23	n_w	ratio between the surface temperature and the fire temperature
24	n_x and n_y	ratios between the internal and surface temperatures due to heating in the x and y directions, respectively
25		
26	P	axial load
27	r	length of descending branch in concrete stress-strain relationship
28	t	fire duration
29	t^*	Equivalent fire duration assuming ISO 834 standard fire
30	T	temperature in degree Celsius [$1\text{ }^\circ\text{F} = 1.8\text{ }^\circ\text{C} + 32$]
31	T_σ	temperature produces the same average concrete strength for the layer
32	T_{th}	algebraic average temperature of the elements within each layer
33	T_{xy}	temperature rise at any point located at (x, y)
34	T_{avg}	algebraic average distribution along the section height
35	$T_{avg 1}$	average temperature for regions affected by heating from either left or right
36	$T_{avg 2}$	average temperature for regions not affected by heating from left or right
37	$T_{avg 3}$	average temperature due to heating from the left and right sides simultaneously
38	T_f	fire temperature
39	T_f (ISO)	ISO 834 standard fire temperature at a modified fire duration t^*
40	x, y	horizontal and vertical coordinates for any point within the column/beam section, origin located at bottom left of the section
41		
42	y_1, y_2	boundaries of internal concrete compression force measured in y direction
43	z	boundary of fire affected regions

1	Z_1, Z_2	constants of average temperature fitting equation, Eq. (7)
2	Z_3, Z_4	constants defining the linear variation of ε_{cT} in y direction, Eq. (15)
3	ε	total concrete strain at elevated temperatures
4	ε_{th}	unrestrained thermal strain of concrete
5	ε_{tr}	transient creep strain in concrete
6	ε_c	instantaneous stress-related strain
7	$\frac{\varepsilon_{cT}}$	equivalent mechanical strain in concrete during fire exposure
8	$\frac{\varepsilon_{th}}$	equivalent linear thermal strain
9	ε_i	unrestrained thermal axial strain
10	ε_{st}	self induced thermal strains
11	ε_{sT}	equivalent mechanical strain in steel during fire exposure
12	ε_o	strain at maximum stress of unconfined concrete at ambient temperature
13	ε_{oT}	value of ε_c at peak stress f'_{cT}
14	ε_{uT}	ultimate compressive strain of concrete, Eq. (10)
15	$\varepsilon_{cT max}$	compression strain corresponding to the flexural capacity
16	$\Delta\varepsilon$	difference between ε_{uT} and $(\varepsilon_{oT} + \varepsilon_{tr})$ equals to 0.02
17	ψ_i	unrestrained thermal curvature
18	λ	axial or flexural load level
19	ρ	reinforcement ratio
20	Γ	compartment time factor
21		
22		

1 References

- 2 [1] Lie, T.T., "Structural Fire Protection", ASCE Manuals and Reports on Engineering
3 Practice, no. 78, New York, NY, 1992, 241 pp.
- 4 [2] Youssef, M.A. Moftah, M., "General stress-strain relationship for concrete at elevated
5 temperatures", Engineering Structures, vol. 29, no. 10, 2007, pp. 2618-2634.
- 6 [3] Lie, T.T., Woollerton, J. L., "Fire resistance of reinforced-concrete columns: Test results",
7 Internal Rep. No. 569, 1998, National Research Council of Canada, Quebec, Canada.
- 8 [4] Lie, T.T., Lin, T.D., Allen, D.E., Abrams, M.S., "Fire resistance of reinforced concrete
9 columns", Technical Paper No. 378, 1984, Division of Building Research, National
10 Research Council of Canada, Ottawa, Ontario, Canada.
- 11 [5] Law, A., Gillie, M., "Interaction diagrams for ambient and heated concrete sections", Eng.
12 Struct., vol. 32, no. 6, 2010, pp. 1641-1649.
- 13 [6] Eurocode 2, "Design of concrete structures", ENV EC2, 1992.
- 14 [7] Raut, N., Kodur, V.K.R., "Modeling the fire response of reinforced concrete columns under
15 biaxial bending", ACI Str. J., vol. 108, no. 6, 2011, pp. 1-24.
- 16 [8] El-Fitiany, S.F., and Youssef, M.A., "Stress Block Parameters for Reinforced Concrete
17 Beams during Fire Events," Innovations in Fire Design of Concrete Structures, ACI SP-
18 279, 2011, pp. 1-39.
- 19 [9] El-Fitiany, S., Youssef, M.A., "Assessing the flexural and axial behaviour of reinforced
20 concrete members at elevated temperatures using sectional analysis", Fire Safety Journal,
21 vol. 44, no. 5, 2009, pp. 691-703.
- 22 [10] El-Fitiany S.F. and Youssef M.A., "A Simplified Sectional Analysis Approach for RC
23 Elements during Fire Events", 6th International Conference on Structures in Fire, Michigan
24 State University in East Lansing, MI, 2010, pp. 239-246.
- 25 [11] Wickstrom, U., "A very simple method for estimating temperature in fire exposed concrete
26 structures", Fire Technology Technical report SP-RAPP 1986, 46, Swedish National
27 Testing Institute, pp. 186-194.
- 28 [12] Terro, M.J., "Numerical modeling of the behavior of concrete structures in fire", ACI
29 Struct. J., vol. 95, no. 2, 1998, pp. 183-193.
- 30 [13] Meda, A., Gambarova, P.G., Bonomi, M., "High-Performance Concrete in Fire-Exposed
31 Reinforced Concrete Sections ", ACI Struct. J., vol. 99, no. 3, 2002, pp. 277-287.
- 32 [14] Elbahy Y.I., Youssef M.A., Nehdi M., "Stress Block Parameters for Concrete Flexural
33 Members Reinforced with Superelastic Shape Memory Alloys", Materials and Structures,
34 vol. 42, no. 10, 2009, pp 1335-1351.
- 35 [15] Caldas, R.B., Sousa Jr., J.B.M., Fakurya, R.H., "Interaction diagrams for reinforced
36 concrete sections subjected to fire", Eng. Struct., vol. 32, no.9, 2010, pp. 2832–2838.

37

38

39

1

Table (1) – Parametric study cases

Col #	b (mm)	h (mm)	f'_c (MPa)	f_y (MPa)	ρ % (A_g)
C1	305	305	36.1	443.7	2.1
C2	400	400	30.0	400.0	1.5
C3	600	600	40.0	400.0	1.5
C4	400	700	50.0	400.0	1.0
C5	500	700	25.0	400.0	1.0

* all columns are analyzed up to 4 hrs of standard
ASTM-E119 fire exposure

2
3
4
5
6
7

8

9

Table (2) – Calculation of steel internal forces

A_s (mm ²)	x (mm)	y (mm)	T_{xy} (°C)	ε_{sT}	$\frac{f_{yT}}{f_y}$	$f [T, 0.001]$ (MPa)	$f [T, (\varepsilon_{sT} - \varepsilon_p + 0.001)]$ (MPa)	f_{sT} (MPa)	P_s (kN)	$P_s \cdot y$ (kN.m)
			Eq. (4)	Eq. (18)	Eq. (16)	Eq. (17d)	Eq. (17e)	Eq. (17a,b)	$f_{sT} \times A_s$	
600	50	50	559	0.029	0.46	65	170	217	130,028	6,501,391
600	133	50	342	0.029	0.77	116	241	325	195,071	9,753,525
600	217	50	342	0.029	0.77	116	241	325	195,071	9,753,525
300	300	50	342	0.029	0.77	116	241	325	97,535	4,876,763
600	50	133	342	0.021	0.77	116	236	320	191,761	25,561,774
600	50	217	342	0.014	0.77	116	225	308	185,048	40,099,867
600	50	300	342	0.007	0.77	116	195	279	167,236	50,170,885
600	50	383	342	-0.001	0.77	116	52	100	-59,970	-22,986,365
600	50	467	342	-0.008	0.77	116	205	289	-173,526	-80,984,368
600	50	550	559	-0.016	0.46	65	153	200	-119,815	-65,898,443
600	133	550	342	-0.016	0.77	116	228	312	-187,129	-102,920,724
600	217	550	342	-0.016	0.77	116	228	312	-187,129	-102,920,724
300	300	550	342	-0.016	0.77	116	228	312	-93,564	-51,460,362

$$\sum P_s = \quad \sum P_s \cdot y =$$

$$340,617 \quad -280,453,254$$

10

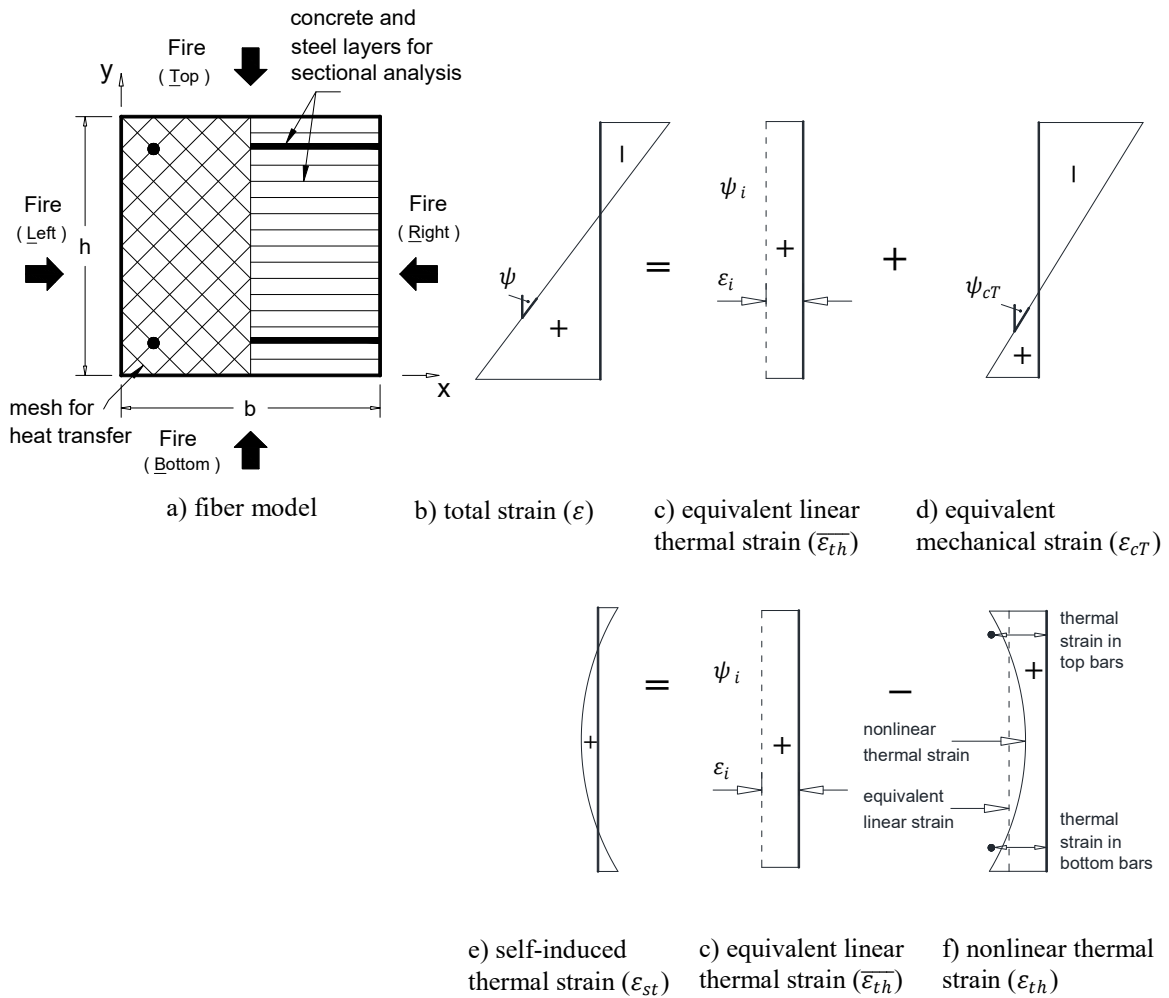


Fig. 1. Sectional analysis approach for a fire-exposed RC columns

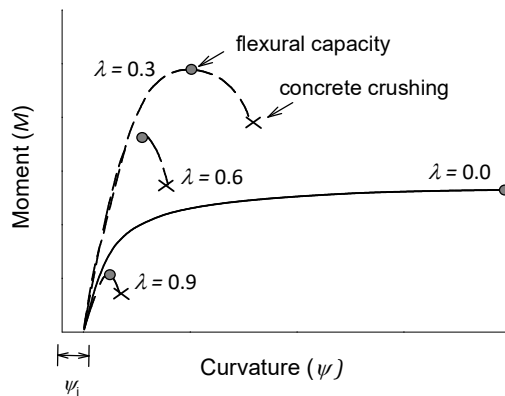


Fig. 2. Schematic M - ψ relationships at different axial load levels

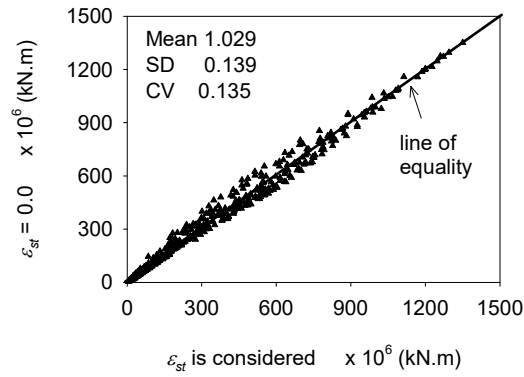


Fig. 3. Effect of ignoring ϵ_{st} on the flexural capacity of fire-exposed columns

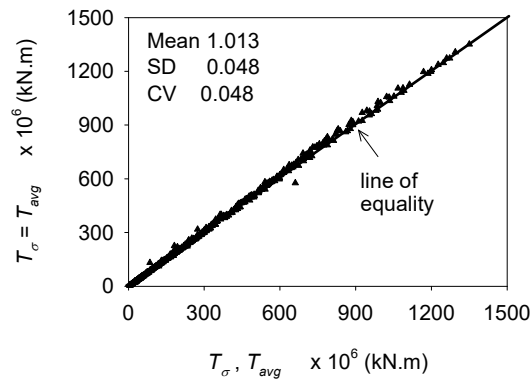


Fig. 4. Effect of neglecting T_σ on the flexural capacity of fire-exposed columns

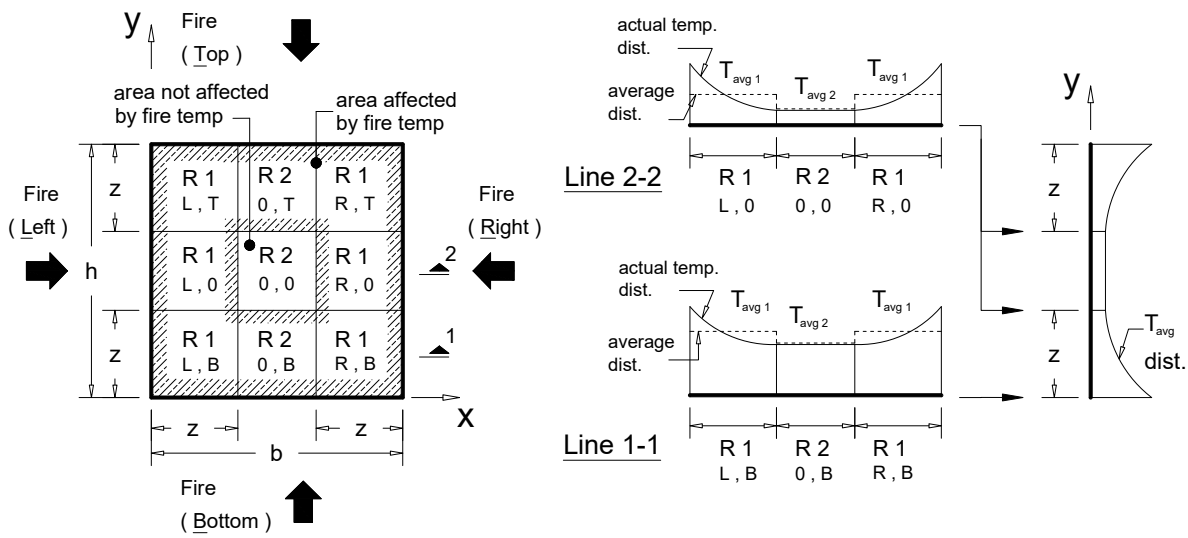


Fig. 5. Temperature calculation of a fire-exposed RC column ($z \leq b/2$)

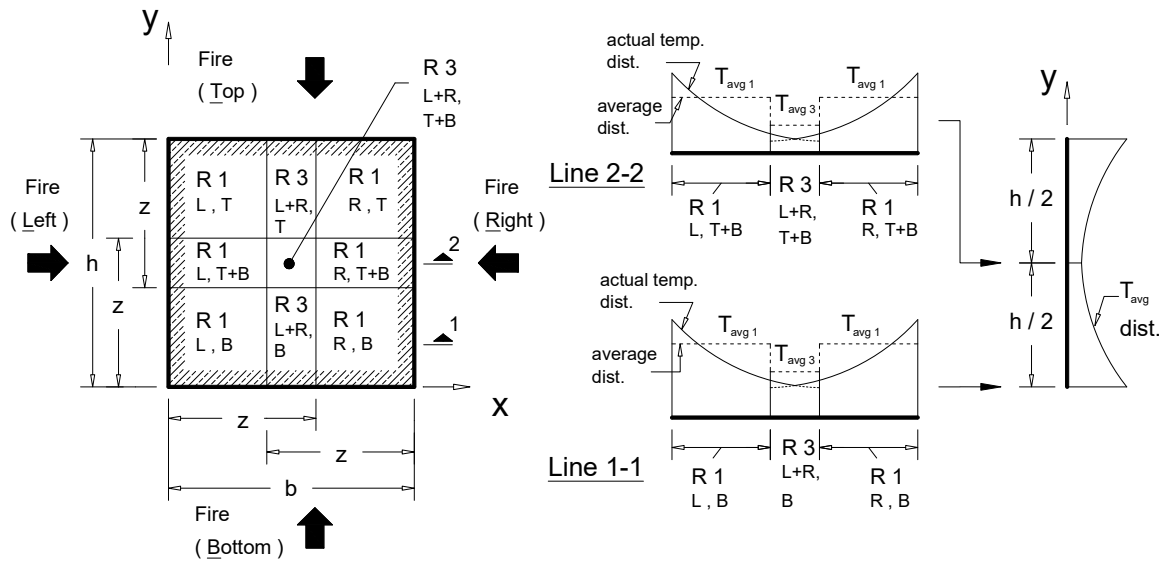


Fig. 6. Temperature calculation of a fire-exposed RC column ($z > b/2$)

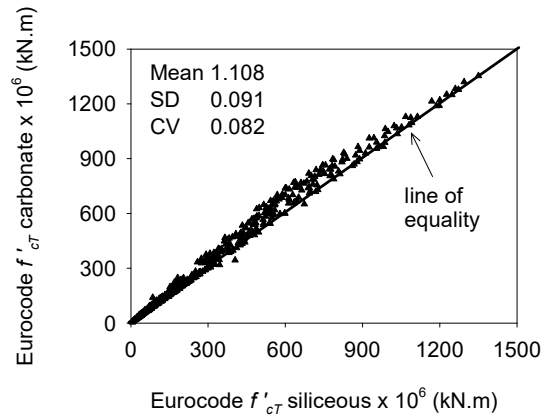


Fig. 7. Effect of aggregate type on the flexural capacity of fire-exposed columns

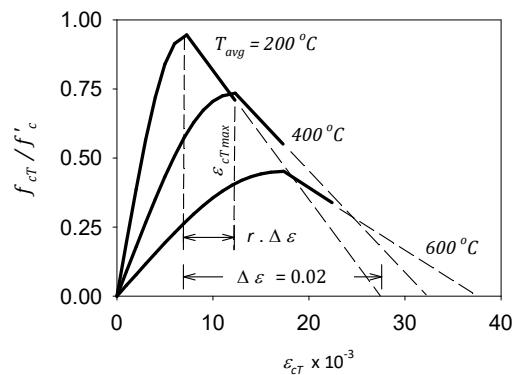


Fig. 8. Concrete stress-strain relationships at different elevated temperatures

1
2
3
4
5
6
7
8
9
10
11
12
13
14
15
16
17
18
19
20
21
22
23
24
25
26
27
28
29
30
31
32
33
34
35
36
37
38
39
40
41
42
43
44
45
46
47

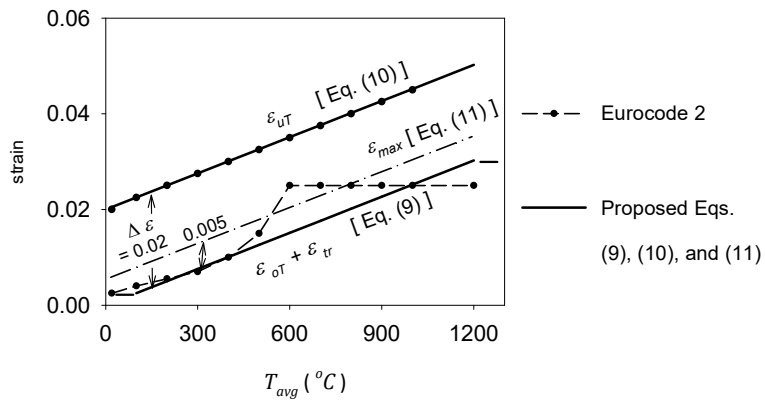


Fig. 9. Variation of $(\varepsilon_{OT} + \varepsilon_{tr})$, ε_{UT} , and $\varepsilon_{CT\ max}$ at elevated temperatures

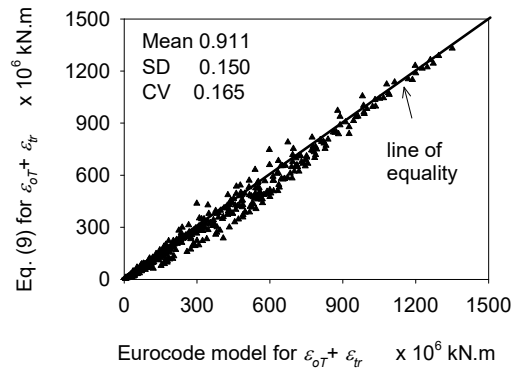


Fig. 10. Effect of using Eq. (9) on the flexural capacity of fire-exposed columns

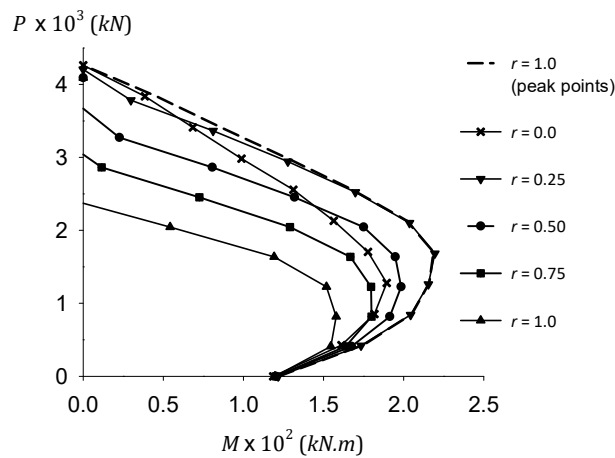


Fig. 11. P - M diagrams for column C2 with using different r values

1
2
3
4
5
6
7
8
9
10
11
12
13
14
15
16
17
18
19
20
21
22
23
24
25
26
27
28
29
30
31
32
33
34
35
36
37
38
39
40
41
42
43
44
45
46
47

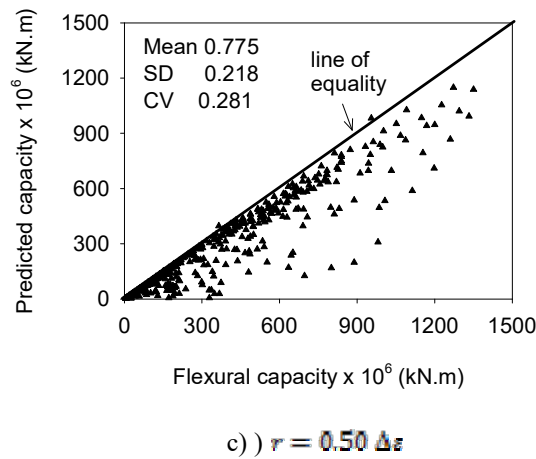
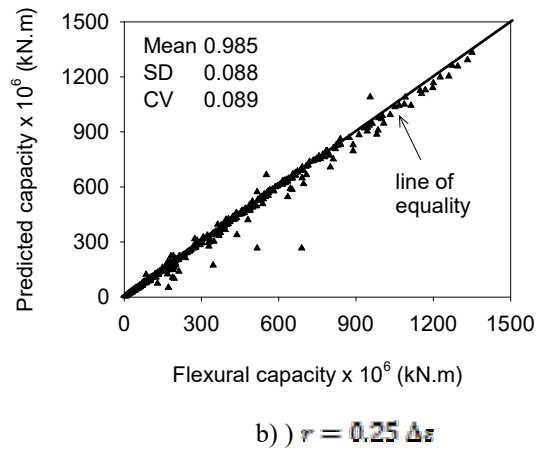
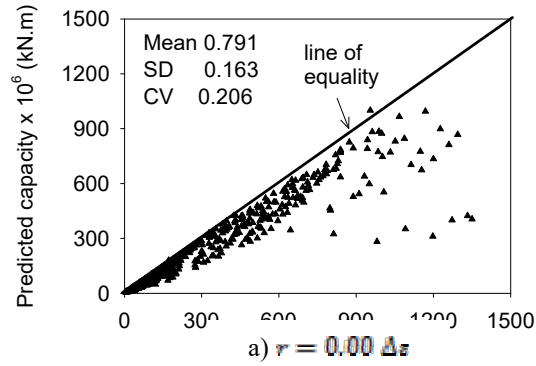


Fig. 12. Effect of descending branch length on flexural capacity

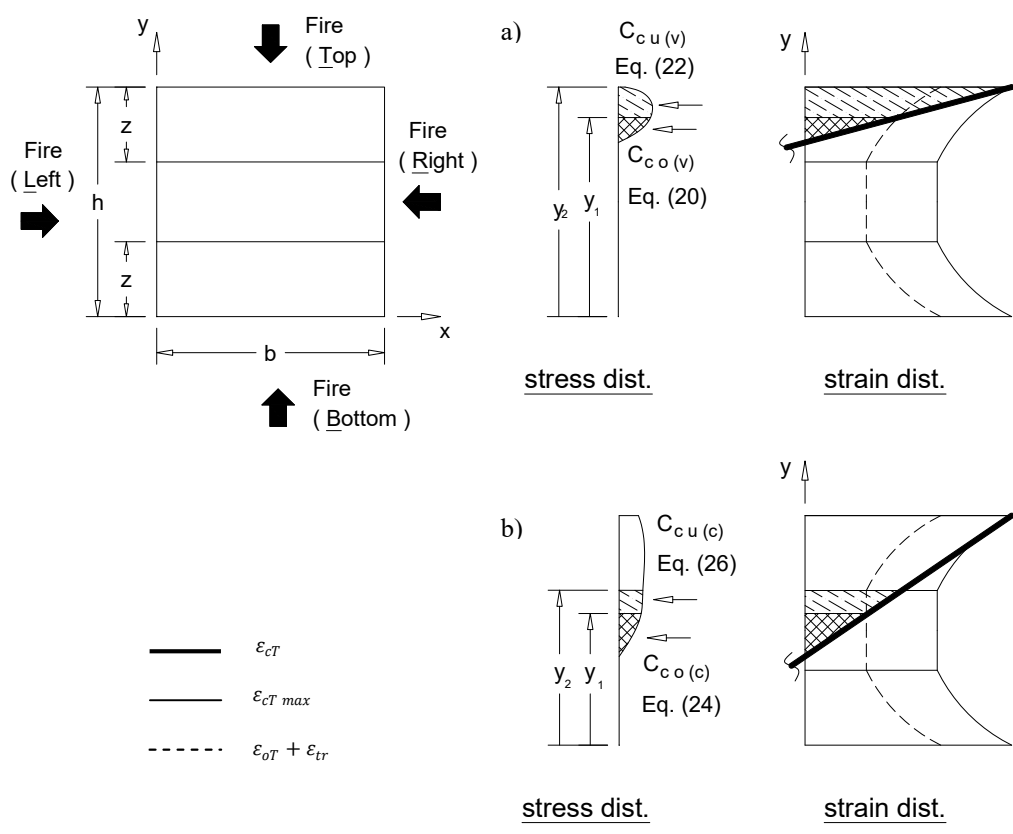


Fig. 13. Different cases for concrete internal compression force

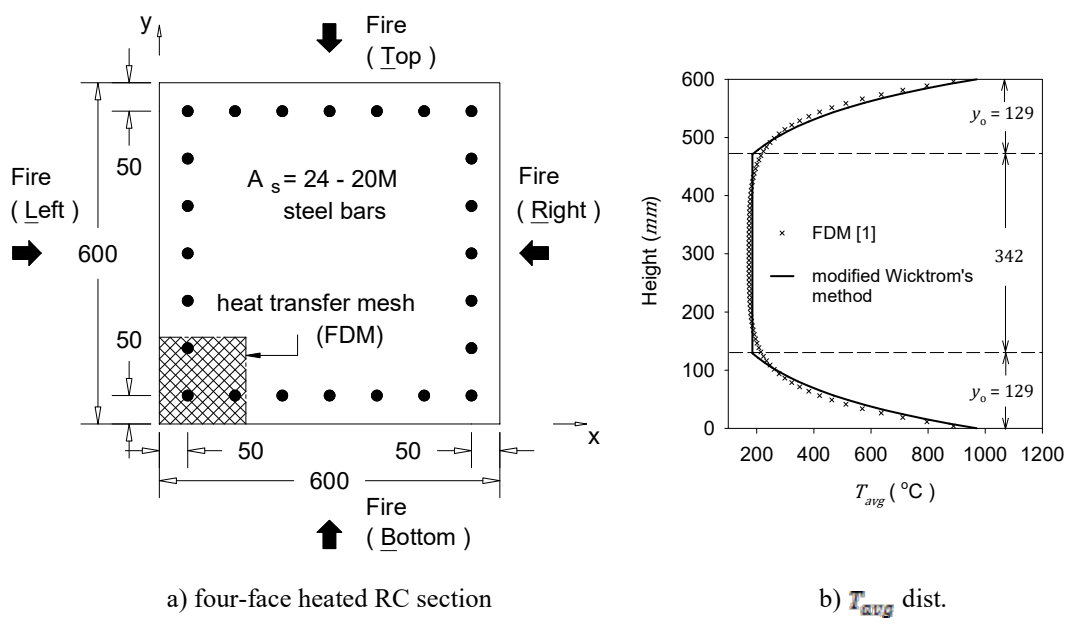


Fig. 14. T_{avg} distribution of example RC column [Dimensions in mm]

1
2
3
4
5
6
7
8
9
10
11
12
13
14
15
16
17
18
19
20
21

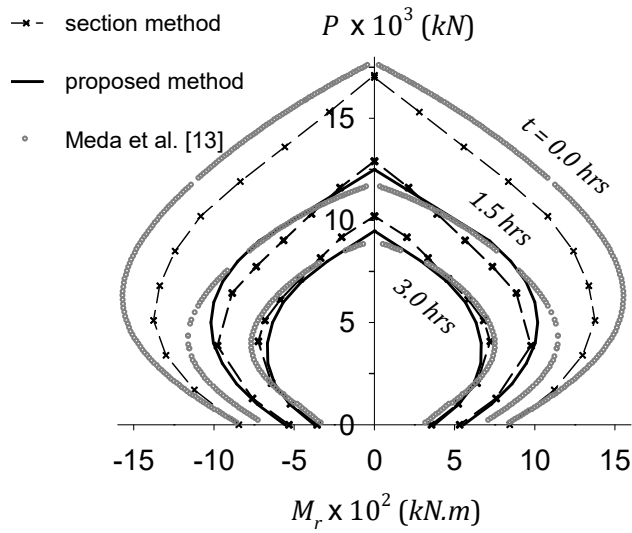


Fig. 15. P - M diagrams for example column

22
23
24
25
26
27
28
29
30
31
32
33
34
35
36
37
38
39
40
41
42
43
44
45

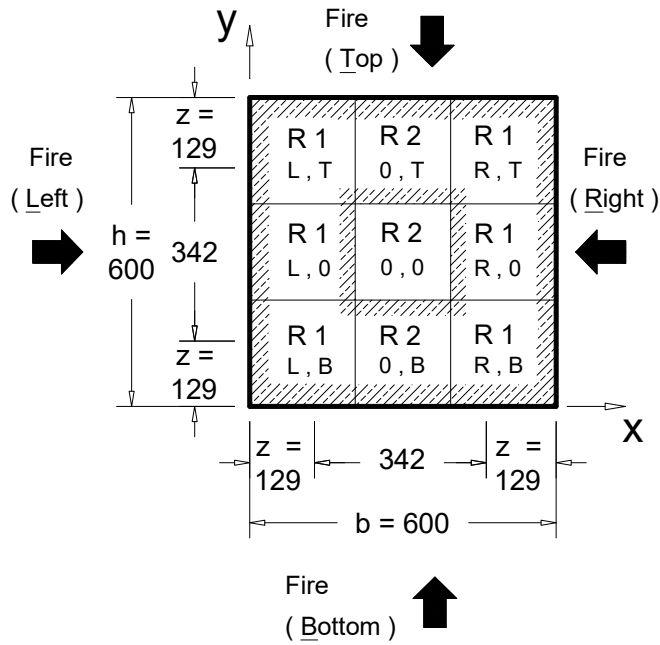


Fig. 16. Temperature calculation of a example column [Dimensions in mm]

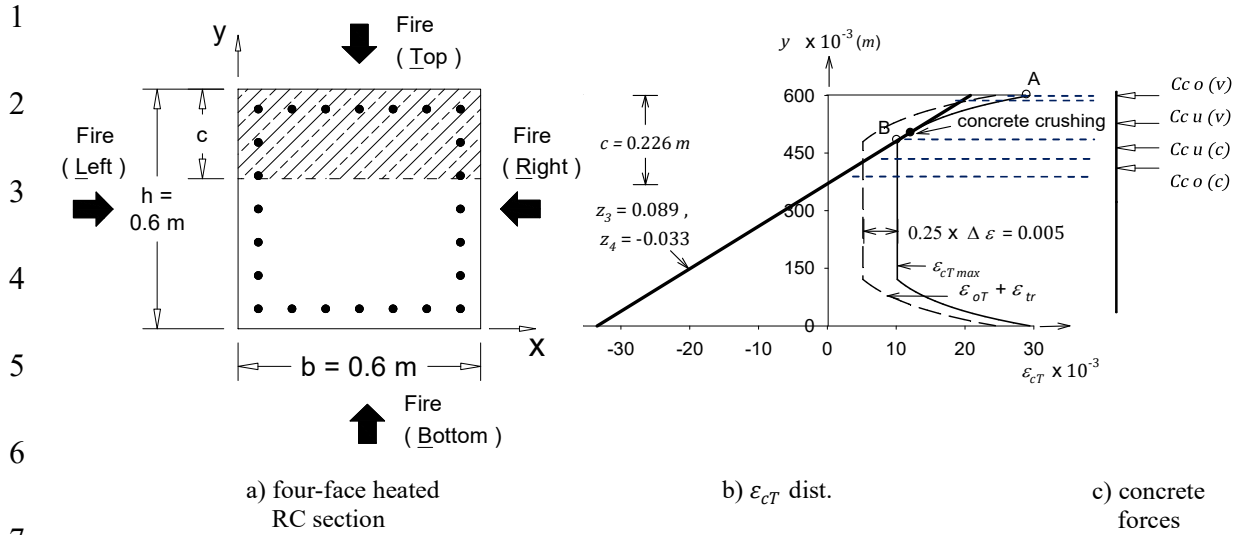


Fig. 17. Concrete internal compression force for example column

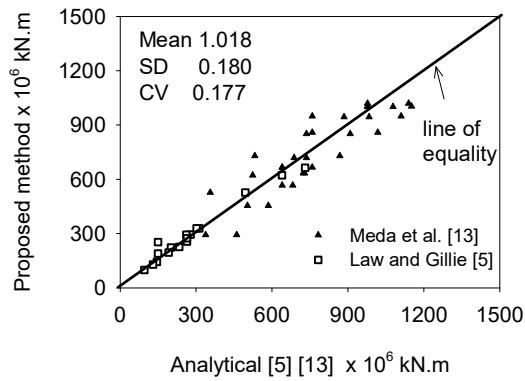


Fig. 18. Flexural capacity predictions of proposed method during fire exposure

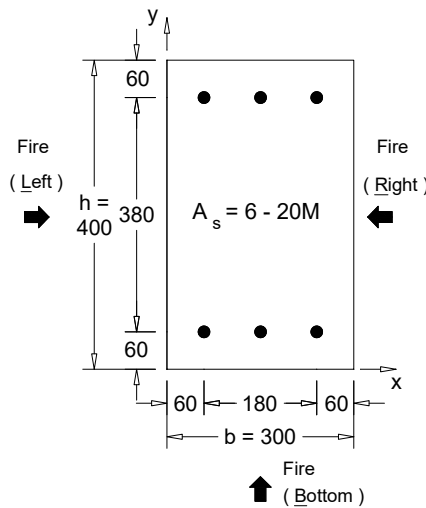


Fig. 19. Column section analyzed by Law and Gillie [5]

1
2
3
4
5
6
7
8
9
10
11
12
13
14
15
16
17
18
19
20
21
22
23
24
25
26
27
28
29
30
31
32
33
34
35
36

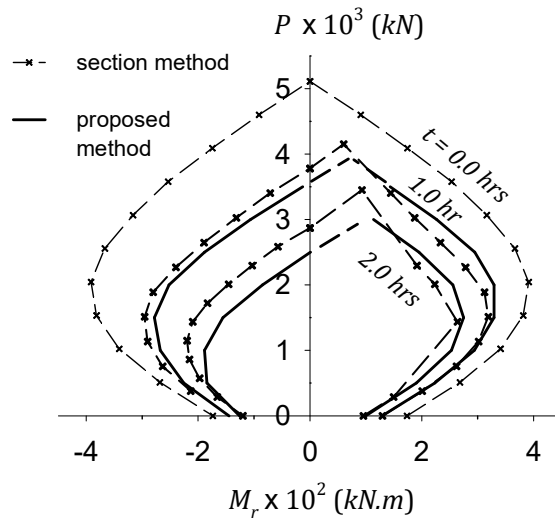


Fig. 20. P - M diagrams for Law and Gillie [5] column

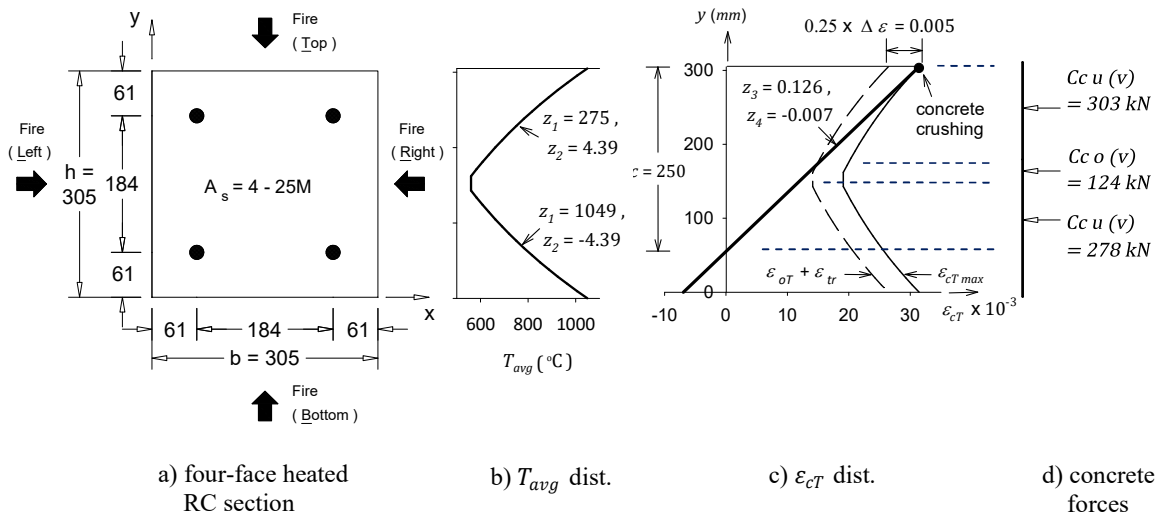


Fig. 21. Concrete internal compression force for Lie and Woollerton [3] column

1 **Appendix I**

2 $C_{c o(v)} = 2 C_{c o(v) L} - C_{c o(v) N}$ (18a)

3

4 $C_{c o(v) L} = \left(\frac{1}{30.465} \frac{b f_c}{z_2^2 z_1} \right) [$ (18b)

5 $-(A_2^2 y_2 - A_1^2 y_1) \times 1065 z_1^3 z_3 z_2 \quad + (A_2 y_2 - A_1 y_1) \times 3630767 z_1^2 z_3 z_2$

6 $+ (A_2^2 - A_1^2) \times 1065 z_1^3 (0.5 z_3 - z_4 z_2) + (A_2 - A_1) \times 3630767 z_1^2 (z_4 z_2 - z_3)$

7 $+ \left(\frac{y_2}{A_2} - \frac{y_1}{A_1} \right) \times 1210.981 \times 10^9 z_3 z_2$

8 $+ \left(\frac{1}{A_2} - \frac{1}{A_1} \right) \times 1210.981 \times 10^9 (z_3 + z_4 z_2)$

9 $-(y_2^2 - y_1^2) \times 1515.812 \times 10^5 z_1 z_3 z_2^2$

10 $-(y_2 - y_1) \times 3031.623 \times 10^5 z_1 z_4 z_2^2]$

11

12

13

14

15

16

17

18

$$\begin{aligned}
1 \quad C_{c o(v) N} &= \left(\frac{5.21026 b f'_c}{z_2^3 z_1^2} \right) [& (18c) \\
2 \quad & + \left(\frac{y_2^2}{A_2^2} - \frac{y_1^2}{A_1^2} \right) \times 1.5137262 \times 10^{14} z_3^2 z_2^2 \\
3 \quad & + \left(\frac{y_2}{A_2^2} - \frac{y_1}{A_1^2} \right) \times 3.0274525 \times 10^{14} (z_3 z_4 z_2^2 + 0.5 z_3^2 z_2) \\
4 \quad & + \left(\frac{1}{A_2^2} - \frac{1}{A_1^2} \right) \times 1.5137262 \times 10^{14} (z_3 z_4 z_2 + 0.5 z_3^2 + z_4^2 z_2^2) \\
5 \quad & + \left(\frac{y_2^2}{A_2} - \frac{y_1^2}{A_1} \right) \times 7.579058 \times 10^{10} z_1 z_3^2 z_2^2 \\
6 \quad & + \left(\frac{y_2}{A_2} - \frac{y_1}{A_1} \right) \times 1.5158116 \times 10^{11} (z_1 z_3^2 z_2 + z_1 z_3 z_4 z_2^2) \\
7 \quad & + \left(\frac{1}{A_2} - \frac{1}{A_1} \right) \times 1.5158116 \times 10^{11} (z_1 z_3 z_4 z_2 + 0.5 z_1 z_4^2 z_2^2 + z_1 z_3^2) \\
8 \quad & - (A_2 y_2^2 - A_1 y_1^2) \times 532.5016 \times 10^3 z_1^3 z_3^2 z_2^2 \\
9 \quad & + (A_2 y_2 - A_1 y_1) \times 1065.0032 \times 10^3 (z_1^3 z_3^2 z_2 - z_1^3 z_3 z_4 z_2^2) \\
10 \quad & + (A_2 - A_1) \times 1065.0032 \times 10^3 (z_1^3 z_3 z_4 z_2 - 0.5 z_1^3 z_4^2 z_2^2 - z_1^3 z_3^2) \\
11 \quad & + (y_2^3 - y_1^3) \times 3.025639 \times 10^8 z_1^2 z_3^2 z_2^3 \\
12 \quad & + (y_2^2 - y_1^2) \times 9.0769173 \times 10^8 z_1^2 z_3 z_2^3 z_4 \\
13 \quad & + (y_2 - y_1) \times 9.0769173 \times 10^8 z_1^2 z_4^2 z_2^3] \\
14 \\
15 \\
16 \\
17 \\
18
\end{aligned}$$

$$1 \quad C_{c o(v)} \cdot y = 2 C_{c o(v) L} \cdot y - C_{c o(v) N} \cdot y \quad (19a)$$

2

$$3 \quad C_{c o(v) L} \cdot y = \left(\frac{1}{9.1395} \frac{b f'_c}{z_2^3 z_1} \right) [\quad (19b)$$

$$4 \quad -(A_2^2 y_2^2 - A_1^2 y_1^2) \times 3195 \times 10^{-4} z_1^3 z_3 z_2^2$$

$$5 \quad +(A_2 y_2^2 - A_1 y_1^2) \times 1.08923 \times 10^3 z_1^2 z_3 z_2^2$$

$$6 \quad +(A_2^2 y_2 - A_1^2 y_1) \times 3195 \times 10^{-4} z_1^3 z_2 (z_3 - z_4 z_2)$$

$$7 \quad +(A_2^2 - A_1^2) \times 15975 \times 10^{-5} z_1^3 (z_4 z_2 - z_3)$$

$$8 \quad +(A_2 y_2 - A_1 y_1) \times 1.08923 \times 10^3 z_1^2 z_2 (-2 z_3 + z_4 z_2)$$

$$9 \quad + \left(\frac{y_2^2}{A_2} - \frac{y_1^2}{A_1} \right) \times 3.632943 \times 10^8 z_3 z_2^2$$

$$10 \quad + \left(\frac{y_2}{A_2} - \frac{y_1}{A_1} \right) \times 3.632943 \times 10^8 (2 z_3 z_2 + z_4 z_2^2)$$

$$11 \quad + \left(\frac{1}{A_2} - \frac{1}{A_1} \right) \times 3.632943 \times 10^8 (2 z_3 + z_4 z_2)$$

$$12 \quad +(A_2 - A_1) \times 1.08923 \times 10^3 (2 z_1^2 z_3 - z_1^2 z_4 z_2)$$

$$13 \quad -(y_2^2 - y_1^2) \times 4.547435 \times 10^4 z_1 z_4 z_2^3 +$$

$$14 \quad -(y_2^3 - y_1^3) \times 3.031623 \times 10^4 z_1 z_3 z_2^3]$$

15

16

17

18

$$\begin{aligned}
1 \quad C_{c o(v) N} \cdot y &= \left(\frac{5.21026 b f_c}{z_2^4 z_1^2} \right) [& (19c) \\
2 \quad &+(y_2^4 - y_1^4) \times 2.2692293 \times 10^5 z_3^2 z_2^4 z_1^2 \\
3 \quad &+ \left(\frac{y_2^3}{A_2^2} - \frac{y_1^3}{A_1^2} \right) \times 1.5137262 \times 10^{11} z_3^2 z_2^3 \\
4 \quad &+(y_2^3 - y_1^3) \times 6.0512782 \times 10^5 z_3 z_2^4 z_4 z_1^2 \\
5 \quad &-(A_2 y_2^3 - A_1 y_1^3) \times 532.5016 z_1^3 z_3^2 z_2^3 \\
6 \quad &+ \left(\frac{y_2^3}{A_2} - \frac{y_1^3}{A_1} \right) \times 7.57906 \times 10^7 z_1 z_3^2 z_2^3 \\
7 \quad &+ \left(\frac{y_2^2}{A_2^2} - \frac{y_1^2}{A_1^2} \right) \times 3.0274525 \times 10^{11} (z_3 z_4 z_2^3 + 0.75 z_3^2 z_2^2) \\
8 \quad &+ \left(\frac{y_2^2}{A_2} - \frac{y_1^2}{A_1} \right) \times 1.5158116 \times 10^5 (1.5 z_1 z_3^2 z_2^2 + z_1 z_3 z_2^3 z_4) \\
9 \quad &+(A_2 y_2^2 - A_1 y_1^2) \times 1065.0032 (1.5 z_1^3 z_3^2 z_2^2 - z_1^3 z_3 z_2^3 z_4) \\
10 \quad &+(y_2^2 - y_1^2) \times 4.5384586 \times 10^5 z_4^2 z_2^4 z_1^2 \\
11 \quad &+(A_2 y_2 - A_1 y_1) \times 532.5016 (4 z_1^3 z_3 z_4 z_2^2 - 6 z_1^3 z_3^2 z_2 - z_1^3 z_4^2 z_2^3) \\
12 \quad &+ \left(\frac{y_2}{A_2^2} - \frac{y_1}{A_1^2} \right) \times 3.0274525 \times 10^{11} (z_3 z_4 z_2^2 + 0.75 z_3^2 z_2 + 0.5 z_4^2 z_2^3) \\
13 \quad &+ \left(\frac{y_2}{A_2} - \frac{y_1}{A_1} \right) \times 0.757906 \times 10^8 (6 z_1 z_3^2 z_2 + 4 z_1 z_3 z_4 z_2^2 + z_1 z_4^2 z_2^3) \\
14 \quad &+ \left(\frac{1}{A_2^2} - \frac{1}{A_1^2} \right) \times 0.756863 \times 10^{11} (1.5 z_3^2 + z_4^2 z_2^2 + 2 z_3 z_4 z_2) \\
15 \quad &+ \left(\frac{1}{A_2} - \frac{1}{A_1} \right) 0.757906 \times 10^8 (4 z_1 z_3 z_4 z_2 + z_1 z_4^2 z_2^2 + 6 z_1 z_3^2) \\
16 \quad &+(A_2 - A_1) \times 532.5016 (-4 z_1^3 z_3 z_4 z_2 + z_1^3 z_4^2 z_2^2 + 6 z_1^3 z_3^2) \\
17 \quad &
\end{aligned}$$

$$\begin{aligned}
1 \quad C_{c u}(v) &= \left(\frac{1}{2.67609} \frac{b f'_c}{z_2^2 \Delta \varepsilon} \right) [& (20) \\
2 \quad &+(y_2^2 - y_1^2) \times 1.3403194 \times 10^6 z_3 z_2^2 \\
3 \quad &+(A_2 y_2 - A_1 y_1) \times 6.71083 \times 10^2 z_1 z_3 z_2 \\
4 \quad &+(A_2^3 y_2 - A_1^3 y_1) \times 1.571667 \times 10^{-3} z_1^3 z_3 z_2 \\
5 \quad &-(A_2^2 y_2 - A_1^2 y_1) \times 4.01855 z_1^2 z_3 z_2 \\
6 \quad &-(A_2^4 - A_1^4) \times 2.97045 \times 10^{-8} z_1^4 z_2 \\
7 \quad &+(A_2^3 - A_1^3) \times (-5.23889 \times 10^{-4} z_1^3 z_3 + 3.607829 \times 10^{-5} z_1^3 z_2 \\
8 \quad &\quad \quad \quad + 1.571667 \times 10^{-3} z_1^3 z_4 z_2) \\
9 \quad &+(A_2^2 - A_1^2) \times 4.01855 (0.5 z_1^2 z_3 - z_1^2 z_4 z_2) \\
10 \quad &+(A_2^2 - A_1^2) \times 7.191535 \times 10^{-2} z_1^2 z_2 \\
11 \quad &+(A_2 - A_1) \times 6.71083 \times 10^2 (-z_1 z_3 + z_1 z_4 z_2) \\
12 \quad &-(A_2 - A_1) \times 80.97376 z_1 z_2] \\
13 \\
14 \\
15 \\
16 \\
17 \\
18 \\
19
\end{aligned}$$

$$\begin{aligned}
1 \quad C_{cu(v)} \cdot y &= \left(\frac{1}{3.2113} \frac{-b f'_c}{z_2^3 \Delta \varepsilon} \right) [& (21) \\
2 \quad & -(y_2^3 - y_1^3) \times 1.0722555 \times 10^3 z_3 z_2^3 \\
3 \quad & +(y_2^2 - y_1^2) \times 32.16767(-50 z_4 z_2^3 + z_2^3) \\
4 \quad & +(A_2^2 y_2^2 - A_1^2 y_1^2) \times 4.82226 \times 10^{-3} z_1^2 z_3 z_2^2 \\
5 \quad & -(A_2^3 y_2^2 - A_1^3 y_1^2) \times 1.886 \times 10^{-6} z_1^3 z_3 z_2^2 \\
6 \quad & -(A_2 y_2^2 - A_1 y_1^2) \times 0.8053 z_1 z_3 z_2^2 \\
7 \quad & +(A_2^2 y_2 - A_1^2 y_1) \times 4.82226 \times 10^{-3}(-z_1^2 z_3 z_2 + z_1^2 z_4 z_2^2) \\
8 \quad & -(A_2^2 y_2 - A_1^2 y_1) \times 8.62984 \times 10^{-5} z_1^2 z_2^2 \\
9 \quad & +(A_2^3 y_2 - A_1^3 y_1) \times 1.257334 \times 10^{-6}(z_1^3 z_3 z_2 - 1.5 z_1^3 z_4 z_2^2) \\
10 \quad & -(A_2^3 y_2 - A_1^3 y_1) \times 4.3294 \times 10^{-8} z_1^3 z_2^2 \\
11 \quad & +(A_2 y_2 - A_1 y_1) \times 0.8053(-z_1 z_4 z_2^2 + 2 z_1 z_3 z_2) \\
12 \quad & +(A_2 y_2 - A_1 y_1) \times 9.7169 \times 10^{-2} z_1 z_2^2 \\
13 \quad & +(A_2^4 y_2 - A_1^4 y_1) \times 3.56454 \times 10^{-11} z_1^4 z_2^2 \\
14 \quad & +(A_2^3 - A_1^3) \times 4.19113 \times 10^{-7}(1.5 z_1^3 z_4 z_2 - z_1^3 z_3) \\
15 \quad & +(A_2^3 - A_1^3) \times 1.4431 \times 10^{-8} z_1^3 z_2 \\
16 \quad & +(A_2 - A_1) \times 0.8053(-0.5 z_1 z_3 + z_1 z_4 z_2) \\
17 \quad & -(A_2 - A_1) \times 9.7169 \times 10^{-2} z_1 z_2 \\
18 \quad & +(A_2^2 - A_1^2) \times 2.4111 \times 10^{-3}(z_1^2 z_3 - z_1^2 z_4 z_2) \\
19 \quad & +(A_2^2 - A_1^2) \times 4.315 \times 10^{-5} z_1^2 z_2 - (A_2^4 - A_1^4) \times 8.911 \times 10^{-12} z_1^4 z_2]
\end{aligned}$$

$$\begin{aligned}
1 \quad C_{c o(c)} &= (-1 \times 10^6 b f'_{cT}) \left[-\frac{1}{3} \frac{z_3^2}{\varepsilon_{oT}^2} (y_2^3 - y_1^3) + \left(\frac{z_3}{\varepsilon_{oT}} - z_4 \frac{z_3}{\varepsilon_{oT}^2} \right) (y_2^2 - y_1^2) + \right. \\
2 \quad &\quad \left. \left(2 \frac{z_4}{\varepsilon_{oT}} - \frac{z_4^2}{\varepsilon_{oT}^2} \right) (y_2 - y_1) \right] \tag{22}
\end{aligned}$$

$$\begin{aligned}
3 \\
4 \quad C_{c o(c)} \cdot y &= (-1 \times 10^3 b f'_{cT}) \left[-\frac{1}{4} \frac{z_3^2}{\varepsilon_{oT}^2} (y_2^4 - y_1^4) + \frac{1}{3} \left(2 \frac{z_3}{\varepsilon_{oT}} - 2 z_4 \frac{z_3}{\varepsilon_{oT}^2} \right) \right. \\
5 \quad &\quad \left. (y_2^3 - y_1^3) + \left(\frac{z_4}{\varepsilon_{oT}} - \frac{z_4^2}{2 \varepsilon_{oT}^2} \right) (y_2^2 - y_1^2) \right] \tag{23}
\end{aligned}$$

$$\begin{aligned}
6 \\
7 \quad C_{c u(c)} &= \left(\frac{-1 \times 10^6 b f'_{cT}}{\Delta \varepsilon} \right) \left[\varepsilon_{uT} (y_2 - y_1) - \frac{1}{2} z_3 (y_2^2 - y_1^2) - z_4 (y_2 - y_1) \right] \tag{24}
\end{aligned}$$

$$\begin{aligned}
8 \\
9 \quad C_{c u(c)} \cdot y &= \left(\frac{-1 \times 10^3 b f'_{cT}}{\Delta \varepsilon} \right) \left[-\frac{1}{3} z_3 (y_2^3 - y_1^3) + \frac{1}{2} (\varepsilon_{uT} - z_4) (y_2^2 - y_1^2) \right] \tag{25}
\end{aligned}$$